Our data reveal an unsuspected role of the prorenin receptor PRR in Wnt/β-catenin signaling and provide evidence that this multifunctional protein interacts with V-ATPase. We propose a mechanism wherein PRR is part of the Wnt receptor complex, acting as a specific adaptor between LRP6 and V-ATPase. Upon Wnt stimulation, this signaling complex is endocytosed, and across the vesicle membrane V-ATPase generates a proton gradient that is essential for LRP6 phosphorylation and hence β-catenin activation. Our results raise intriguing questions about the role of PRR in renin signaling and mental retardation and the immediate consequence of acidification in Wnt receptor signaling. The Na^+-H^+ exchanger Nhe2 is required for Fz–planar cell polarity signaling in *Drosophila* (*32*), suggesting that electrochemical regulation may have multiple roles in Wnt receptor signaling. The V-ATPase may also provide a therapeutic target to modulate Wnt signaling in a disease context.

References and Notes

1. P. Polakis, *Genes Dev.* **14**, 1837 (2000).
2. C. Y. Logan, R. Nusse, *Annu. Rev. Cell Dev. Biol.* **20**, 781 (2004).
3. R. T. Moon, A. D. Kohn, G. V. De Ferrari, A. Kaykas, *Nat. Rev. Genet.* **5**, 691 (2004).
4. H. Clevers, *Cell* **127**, 469 (2006).
5. J. Bilic *et al.*, *Science* **316**, 1619 (2007).
6. G. Davidson *et al.*, *Nature* **438**, 867 (2005).
7. X. Zeng *et al.*, *Nature* **438**, 873 (2005).
8. X. Zeng *et al.*, *Development* **135**, 367 (2008).
9. J. Mao *et al.*, *Mol. Cell* **7**, 801 (2001).
10. Materials and methods are available as supporting material on *Science* Online.
11. V. Korinek *et al.*, *Science* **275**, 1784 (1997).
12. G. Nguyen *et al.*, *J. Clin. Investig.* **109**, 1417 (2002).
13. J. J. Saris *et al.*, *Hypertension* **48**, 564 (2006).
14. Y. Huang, N. A. Noble, J. Zhang, C. Xu, W. A. Border, *Kidney Int.* **72**, 45 (2007).
15. M. Sakoda *et al.*, *Hypertens. Res.* **30**, 1139 (2007).
16. A. Contrepas *et al.*, *Am. J. Physiol. Regul. Integr. Comp. Physiol.* **297**, R250 (2009).
17. J. Ramser *et al.*, *Hum. Mol. Genet.* **14**, 1019 (2005).
18. D. J. Campbell, *Hypertension* **51**, 1259 (2008).
19. A. Amsterdam *et al.*, *Proc. Natl. Acad. Sci. U.S.A.* **101**, 12792 (2004).
20. C. Kiecker, C. Niehrs, *Development* **128**, 4189 (2001).
21. A. P. McMahon, A. L. Joyner, A. Bradley, J. A. McMahon, *Cell* **69**, 581 (1992).
22. L. L. McGrew, K. Takemaru, R. Bates, R. T. Moon, *Mech. Dev.* **87**, 21 (1999).
23. J. Ludwig *et al.*, *J. Biol. Chem.* **273**, 10939 (1998).
24. M. Forgac, *Nat. Rev. Mol. Cell Biol.* **8**, 917 (2007).
25. V. Marshansky, M. Futai, *Curr. Opin. Cell Biol.* **20**, 415 (2008).
26. K. W. Beyenbach, H. Wieczorek, *J. Exp. Biol.* **209**, 577 (2006).
27. J. T. Blitzer, R. Nusse, *BMC Cell Biol.* **7**, 28 (2006).
28. H. Yamamoto, H. Komekado, A. Kikuchi, *Dev. Cell* **11**, 213 (2006).
29. A. George, H. Leahy, J. Zhou, P. J. Morin, *Neurobiol. Dis.* **26**, 125 (2007).
30. M. Lu *et al.*, *J. Biol. Chem.* **277**, 38409 (2002).
31. G. Miesenböck, D. A. De Angelis, J. E. Rothman, *Nature* **394**, 192 (1998).
32. M. Simons *et al.*, *Nat. Cell Biol.* **11**, 286 (2009).

33. We thank H. Clevers, R. Grosschedl, X. He, R. Moon, J. Nathans, R. Nusse, M. Levin, G. Miesenböck, Y. M. Chan, M. A. Skinner, and M. Lorizate for reagents; Y. L. Huang for confocal microscopy; A. Glinka for recombinant Wnt3a-V5; and T. Büchling and K. Bartscherer for sharing data before publication and discussion. This work was supported by the Deutsche Forschungsgemeinschaft and the European Commission (Endotrack and Marie-Curie Program). S.P.A. is a recipient of a fellowship from Gobierno Vasco.

Supporting Online Material

www.sciencemag.org/cgi/content/full/327/5964/459/DC1
Materials and Methods
Figs. S1 to S13
Table S1
References
Movie S1

28 July 2009; accepted 4 December 2009
10.1126/science.1179802

Identification of RACK1 and Protein Kinase Cα as Integral Components of the Mammalian Circadian Clock

Maria S. Robles,*† Cyril Boyault,* Darko Knutti,*‡ Kiran Padmanabhan, Charles J. Weitz§

At the core of the mammalian circadian clock is a negative feedback loop in which the dimeric transcription factor CLOCK-BMAL1 drives processes that in turn suppress its transcriptional activity. To gain insight into the mechanisms of circadian feedback, we analyzed mouse protein complexes containing BMAL1. Receptor for activated C kinase–1 (RACK1) and protein kinase C–α (PKCα) were recruited in a circadian manner into a nuclear BMAL1 complex during the negative feedback phase of the cycle. Overexpression of RACK1 and PKCα suppressed CLOCK-BMAL1 transcriptional activity, and RACK1 stimulated phosphorylation of BMAL1 by PKCα in vitro. Depletion of endogenous RACK1 or PKCα from fibroblasts shortened the circadian period, demonstrating that both molecules function in the clock oscillatory mechanism. Thus, the classical PKC signaling pathway is not limited to relaying external stimuli but is rhythmically activated by internal processes, forming an integral part of the circadian feedback loop.

Circadian clocks are oscillators that drive daily biological rhythms. In mammals, circadian clocks are intrinsic to most tissues (*1*, *2*). At the core of the clock is a negative feedback loop (*3*) in which the dimeric transcription factor CLOCK-BMAL1 (*4*) drives transcription of *Period* (*Per*) and *Cryptochrome* (*Cry*) genes. PER and CRY proteins in turn enter the nucleus and suppress CLOCK-BMAL1 activity by an unknown mechanism. Phosphorylation of CLOCK and BMAL1 appears to be important in circadian feedback, affecting CLOCK-BMAL1 activity and/or stability (*5*–*8*). Degradation of PERs and CRYs (*9*–*12*) derepresses CLOCK-BMAL1 activity, initiating a new cycle.

To gain insight into circadian clock negative feedback, we searched for proteins in a complex with BMAL1 at the time when CLOCK-BMAL1 activity was suppressed. BMAL1 complexes, extracted from mouse fibroblasts [BLi cells (*13*)] or tissues collected during the phase of negative feedback, were initially characterized by sucrose density gradient centrifugation. The majority of BMAL1 was in complexes of 200 to 400 kD, but some was in larger complexes, particularly in the liver (fig. S1A).

For isolation of BMAL1 complexes, we used FH-BMAL1, a tagged BMAL1 with a FLAG-hemagglutinin (FH) tandem epitope (*14*) at the N terminus (fig. S1B). Stably expressed FH-BMAL1 [EFH cells (*13*)] was similar to BMAL1 in transcriptional activity and in suppression by CRY1 (fig. S2A), and it was mostly in complexes of 200 to 400 kD (Fig. 1A). FH-BMAL1 thus preserved the basic transcriptional and biochemical properties of BMAL1.

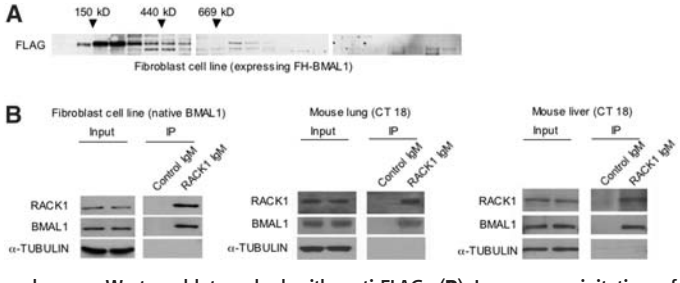

Fig. 1. Identification of RACK1 as a component of a BMAL1 protein complex by proteomics analysis. (**A**) Sucrose density gradient sedimentation (5 to 45% sucrose, from left to right) of FH-BMAL1 protein complexes from mouse fibroblasts stably expressing FH-BMAL1. Image shows a Western blot probed with anti-FLAG. (**B**) Immunoprecipitation of endogenous BMAL1 with endogenous RACK1. Extracts from fibroblasts, liver, or lung (input) and proteins immunoprecipitated (IP) with antibody to RACK1 or control IgG were probed with antibodies to RACK1, BMAL1, and α-TUBULIN, as indicated. CT, circadian time.

Department of Neurobiology, Harvard Medical School, Boston, MA 02115, USA.

*These authors contributed equally to this work.
†Present address: Proteomics and Signal Transduction, Max Planck Institute for Biochemistry, D-82152 Martinsried, Germany.
‡Present address: DSM Nutritional Products, Basel 4002, Switzerland.
§To whom correspondence should be addressed. E-mail: cweitz@hms.harvard.edu

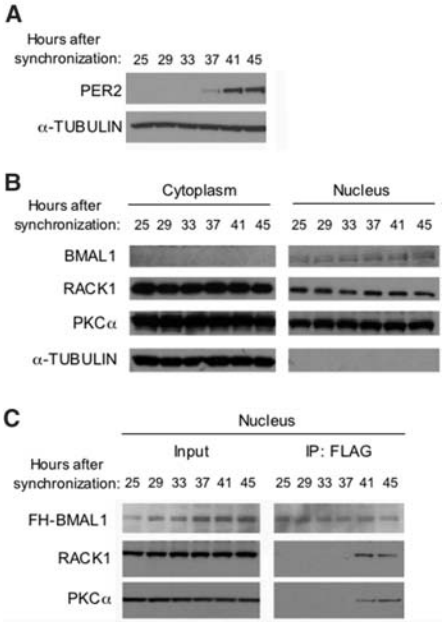

Fig. 2. Circadian association of RACK1 and PKCα with BMAL1 in cell nuclei. (**A**) Coherent circadian rhythms in cultured mouse fibroblasts after synchronization with forskolin. Shown are Western blots analyzing PER2 or α-TUBULIN in extracts of whole cells harvested at 4-hour intervals across a circadian cycle (harvest times indicated at the top). (**B**) Western blot analyzing subcellular and temporal regulation of the indicated proteins. α-TUBULIN, a cytoplasmic marker, serves as control for fractionation. (**C**) Immunoprecipitation (IP) showing a circadian rhythm of association of RACK1 and PKCα with BMAL1 in the nucleus.

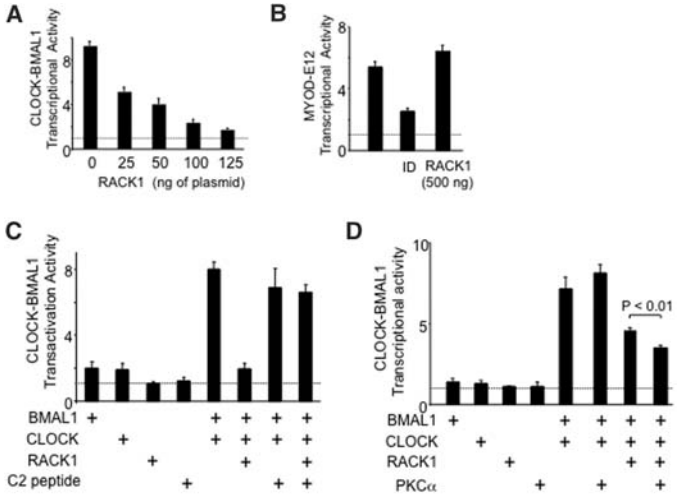

Fig. 3. Inhibition of CLOCK-BMAL1 transcriptional activity by RACK1. (**A**) Effect of RACK1 on CLOCK-BMAL1 transactivation of a luciferase reporter from *Per1* E-boxes (mean ±SD; $N \geq 3$). Mean luciferase activity after transfection of expression vector without inserts was set to 1 (dashed line). (**B**) Effect of RACK1 or ID on MYOD-E12 transactivation of a luciferase reporter from *Mck* gene E-boxes. Data displayed as in (A). (**C**) Antagonization of the inhibitory effect of RACK1 on CLOCK-BMAL1 transcriptional activity by C2 peptide. Displayed as in (A). +, transfection of expression plasmid with insert encoding the indicated protein. (**D**) Partial inhibition of CLOCK-BMAL1 transcriptional activity by RACK1 enhanced by PKCα. Displayed as in (A).

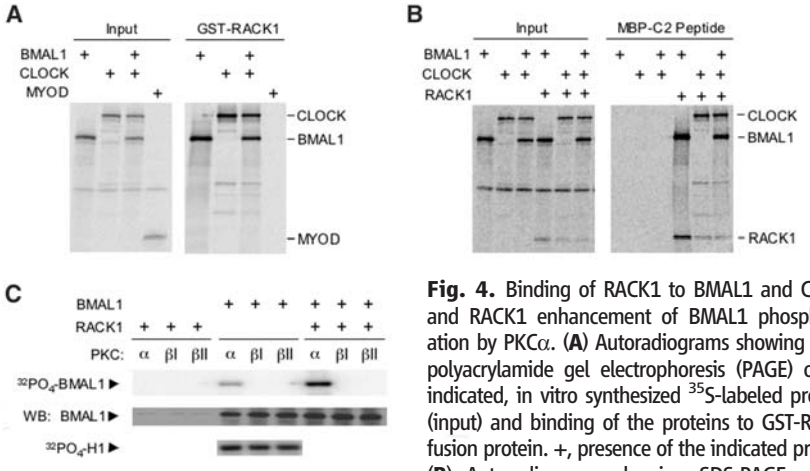

Fig. 4. Binding of RACK1 to BMAL1 and CLOCK and RACK1 enhancement of BMAL1 phosphorylation by PKCα. (**A**) Autoradiograms showing SDS–polyacrylamide gel electrophoresis (PAGE) of the indicated, in vitro synthesized ^{35}S-labeled proteins (input) and binding of the proteins to GST-RACK1 fusion protein. +, presence of the indicated protein. (**B**) Autoradiograms showing SDS-PAGE of the indicated, in vitro synthesized ^{35}S-labeled proteins (input) and binding of the proteins to MBP-C2 fusion protein. Data displayed as in (A). (**C**) Top: Autoradiogram showing in vitro transfer of ^{32}P-labeled phosphate to BMAL1 by the indicated activated PKCs. +, addition of the indicated protein. Middle: Control Western blot documenting BMAL1 in the samples. Bottom: Control autoradiogram showing phosphorylation of histone 1 (H1) by all PKCs.

To identify BMAL1-associated proteins by mass spectrometry, we infected *Bmal1*$^{-/-}$ fibroblasts [MLi cells (*13*)] with either an adenovirus expression vector with no insert (control) or a vector encoding FH-BMAL1. The cells were synchronized, harvested during the phase of negative feedback, and processed for affinity purification of FH-BMAL complexes and subsequent mass spectrometry (fig. S2B). After removing background proteins found in the control, the two proteins from which the most numerous peptides were identified were FH-BMAL1 and CLOCK. Next was RACK1 (receptor for activated C kinase–1), a signaling protein best known for recruiting activated, Ca^{2+}-sensitive protein kinase C (PKC) isoforms, particularly PKCβII but also PKCα and others, to their substrates (*15*–*17*).

To determine whether endogenous BMAL1 and RACK1 are in a complex, we harvested mouse fibroblasts, lung, and liver during the negative feedback phase, immunoprecipitated RACK1, and probed for BMAL1. Endogenous BMAL1 from all sources coimmunoprecipitated with endogenous RACK1 (Fig. 1B), indicating that the two proteins are associated in multiple tissues.

We monitored BMAL1, RACK1, and PKCα expression across the circadian cycle, the latter because of its role in resetting the suprachiasmatic nucleus (SCN) clock (*18*). After synchronization, fibroblasts exhibited the expected circadian rhythm of PER2 (Fig. 2A). The cells were harvested at six time points and separated into cytoplasmic and nuclear fractions, which were then analyzed by Western blotting (Fig. 2B). BMAL1 was mostly nuclear, and RACK1 and PKCα were present in the cytoplasm and nucleus, with little or no circadian variation.

To examine circadian association of the proteins, we harvested synchronized fibroblasts stably expressing FH-BMAL1 at six circadian time points and immunoprecipitated FH-BMAL1 from nuclear fractions (Fig. 2C). BMAL1, RACK1, and PKCα were constitutively present in the nucleus (Fig. 2C, input), but coimmunoprecipitation of RACK1 and PKCα with BMAL1 was detected only during part of the cycle (Fig. 2C), the time corresponding to the phase of negative feedback (see Fig. 2A). Thus, RACK1 and PKCα are components of BMAL1 nuclear complexes, and the formation and/or dissociation of these complexes is under circadian control. Further analysis indicated that RACK1 and PKCα were present in ~400-kD BMAL1 complexes (fig. S3) (*13*).

To test whether RACK1 and PKCα might be negative feedback regulators of CLOCK-BMAL1, as suggested by the time of their association with BMAL1, we assayed the transcriptional activity of CLOCK-BMAL1 (*4*). Cotransfection of increasing amounts of RACK1 expression plasmid negatively correlated with CLOCK-BMAL1 activity

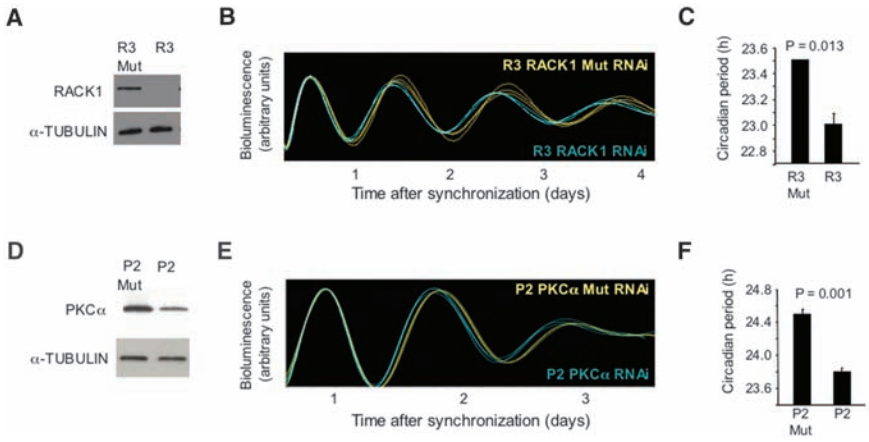

Fig. 5. Short circadian period length caused by depletion of endogenous RACK1 or endogenous PKCα. (**A** to **C**) RACK1; (**D** to **F**) PKCα. (A) Western blot showing the effect of control shRNA (R3 Mut, three point mutations in 22-nucleotide core sequence) or RACK1 shRNA (R3) on steady-state level of endogenous RACK1. α-TUBULIN, loading control. (B) Real-time circadian oscillations of bioluminescence in synchronized circadian reporter fibroblasts after adenoviral delivery of R3 shRNA against RACK1 (blue) or R3 Mut control shRNA (yellow). Traces from three independent cultures are shown for each shRNA. (C) Circadian period of fibroblasts expressing R3 Mut control or R3 RACK1 shRNA (mean ± SEM; $N = 3$ for each; t test, two-tailed). [(D) to (F)] Data for electroporation of control siRNA (P2 Mut, three point mutations in 22-nucleotide core sequence) or effective PKCα siRNA (P2) into fibroblasts displayed as in (A) to (C).

(Fig. 3A). RACK1 produced no inhibition of the activity of MYOD-E12, a transcription factor related to CLOCK-BMAL1 (Fig. 3B).

We tested whether this effect of RACK1 likely involved PKC. C2 is a loop of PKCβII (nearly identical to PKCα) that interacts with RACK1; binding of C2 to RACK1 antagonizes PKC-dependent functions of RACK1 (*19*). Expression of C2 had no effect on either baseline transcription or CLOCK-BMAL1 activity, but C2 reversed the inhibitory action of RACK1 (Fig. 3C). Thus, inhibition of CLOCK-BMAL1 activity by RACK1 likely requires binding of PKC. In addition, expression of PKCα produced no effect on baseline transcription or CLOCK-BMAL1 activity, but it enhanced a partial inhibitory action of RACK1 (Fig. 3D*)*. These results suggest that RACK1 inhibits CLOCK-BMAL1 activity by recruiting PKCα.

RACK1 targets the transcription factor hypoxia-inducible factor–1α (HIF-1α) for degradation (*20*). But from our results (fig. S4) (*13*), it appears that any effect of RACK1 on the steady-state abundance of CLOCK or BMAL1 is unlikely to account for its inhibition of CLOCK-BMAL1 activity.

We analyzed in vitro binding of [^{35}S] methionine-labeled BMAL1, CLOCK, or MYOD to glutathione-*S*-transferase (GST)–RACK1. Both BMAL1 and CLOCK bound to RACK1 fusion protein, whereas the related transcription factor MYOD showed no detectable binding (Fig. 4A). We also examined [^{35}S]methionine-labeled BMAL1, CLOCK, or RACK1, alone or in combination, for binding to a fusion protein of maltose binding protein (MBP) with C2. BMAL1 and CLOCK associated with C2 fusion protein only if RACK1 was present (Fig. 4B). This result suggests that RACK1 promotes assembly of activated PKCα and CLOCK-BMAL1 into a complex.

To determine whether RACK1 might enhance phosphorylation of BMAL1 by PKCα, we synthesized BMAL1 and RACK1 by in vitro transcription-translation and tested the ability of several activated classical PKCs to phosphorylate BMAL1 in vitro with or without RACK1. PKCα, but not PKCβI or PKCβII, phosphorylated BMAL1, and this activity was increased by the presence of RACK1 (Fig. 4C).

If RACK1 has a nonredundant role in the clock, then depletion of endogenous RACK1 should alter circadian period length. We introduced small hairpin RNA constructs (shRNAs) into circadian bioluminescence reporter fibroblasts (*13*) to deplete RACK1. Three nonoverlapping shRNAs each caused depletion of endogenous RACK1 relative to their respective mutated controls (Fig. 5A and fig. S5, A and D), and each caused a shortening of circadian period length observable in individual bioluminescence traces: At the outset, all traces were aligned, but by the second circadian cycle all blue traces (effective RACK1 shRNA) were running ahead of all yellow traces (ineffective mutated shRNA) (Fig. 5B and fig. S5, B and E). The short-period phenotype was significant in all cases (Fig. 5C and fig. S5, C and F).

If a major function of RACK1 in the clock is to recruit PKCα to CLOCK-BMAL1, then depleting PKCα should cause a short-period phenotype like that caused by depletion of RACK1. Three nonoverlapping small interfering double-stranded RNAs (siRNAs) (P1, P2, and P3) were electroporated separately into circadian reporter fibroblasts, and each caused moderate depletion of endogenous PKCα and a significant shortening of circadian period (Fig. 5, D to F, and fig. S6). Thus, RACK1 and PKCα function in the oscillatory mechanism of the clock, and the similar effect of depletion of the two proteins supports the hypothesis that they act in concert.

RACK1 has been identified as a PER1-interacting protein in a yeast two-hybrid screen (*21*), but the in vivo relevance of this finding is unknown. One or more classical PKCs contributes to light-dependent resetting of the SCN clock (*18*, *22*, *23*) and to serum shock resetting of the fibroblast clock (*24*). Mutant mice lacking PKCα have impaired light-dependent resetting of circadian behavioral rhythms, but they exhibit no change in circadian period (*18*). This difference from our results could reflect developmental compensation in the mutant mice, differences between the circadian clocks of the fibroblast and SCN, or, perhaps most likely, the ability of the SCN multioscillator network to compensate for mutations that alter clock function in individual cells (*25*).

Our results indicate that a classical, Ca^{2+}-sensitive signaling pathway is not limited to relaying external stimuli but is triggered by internal processes, forming an integral part of the circadian clock feedback loop. We do not know how this pathway is rhythmically activated, but it is intriguing that circadian oscillations of free Ca^{2+} have been widely observed (*26*, *27*).

References and Notes

1. A. Balsalobre, F. Damiola, U. Schibler, *Cell* **93**, 929 (1998).
2. S. Yamazaki *et al.*, *Science* **288**, 682 (2000).
3. J. S. Takahashi, H. K. Hong, C. H. Ko, E. L. McDearmon, *Nat. Rev. Genet.* **9**, 764 (2008).
4. N. Gekakis *et al.*, *Science* **280**, 1564 (1998).
5. T. Tamaru *et al.*, *Genes Cells* **8**, 973 (2003).
6. H. Dardente, E. E. Fortier, V. Martineau, N. Cermakian, *Biochem. J.* **402**, 525 (2007).
7. T. Tamaru *et al.*, *Nat. Struct. Mol. Biol.* **16**, 446 (2009).
8. H. Yoshitane *et al.*, *Mol. Cell. Biol.* **29**, 3675 (2009).
9. L. Busino *et al.*, *Science* **316**, 900 (2007); published online 26 April 2007 (10.1126/science.1141194).
10. S. M. Siepka *et al.*, *Cell* **129**, 1011 (2007).
11. S. I. H. Godinho *et al.*, *Science* **316**, 897 (2007); published online 26 April 2007 (10.1126/science.1141138).
12. G. Asher *et al.*, *Cell* **134**, 317 (2008).
13. See supporting material on *Science* Online.
14. Y. Nakatani, V. Ogryzko, *Methods Enzymol.* **370**, 430 (2003).
15. D. Schechtman, D. Mochly-Rosen, *Oncogene* **20**, 6339 (2001).
16. H. S. Lee *et al.*, *Osteoarthritis Cartilage* **10**, 890 (2002).
17. E. H. Sklan, E. Podoly, H. Soreq, *Prog. Neurobiol.* **78**, 117 (2006).
18. V. Jakubcakova *et al.*, *Neuron* **54**, 831 (2007).
19. E. G. Stebbins, D. Mochly-Rosen, *J. Biol. Chem.* **276**, 29644 (2001).
20. Y. V. Liu, G. L. Semenza, *Cell Cycle* **6**, 656 (2007).
21. L. Hu *et al.*, *J. Mol. Neurosci.* **29**, 55 (2006).
22. K. M. Schak, M. E. Harrington, *Brain Res.* **840**, 158 (1999).
23. B. Lee, A. Almad, G. Q. Butcher, K. Obrietan, *Eur. J. Neurosci.* **26**, 451 (2007).
24. H. S. Shim *et al.*, *EMBO Rep.* **8**, 366 (2007).
25. A. C. Liu *et al.*, *Cell* **129**, 605 (2007).
26. T. Imaizumi, J. I. Schroeder, S. A. Kay, *Sci. STKE* **2007**, pe32 (2007).

27. M. C. Harrisingh, Y. Wu, G. A. Lnenicka, M. N. Nitabach, *J. Neurosci.* **27**, 12489 (2007).

28. We thank P. Nakatani (Dana-Farber Cancer Institute) for the FH cassette; P. Sassone-Corsi (University of California, Irvine) for BMAL1 antiserum; M. J. Weber (University of Virginia), D. Mochly-Rosen (Stanford University), P. Blumberg (National Cancer Institute), and M. Grossi (University of Rome), respectively, for RACK1, C2, PKCα, and MYOD cDNAs; M. Liu for expert technical assistance; N. Vujovic for help with transactivation assays; and L. Lande-Diner for comments on the manuscript. Supported by grants from the Edward R. and Anne G. Lefler Center and the G. Harold and Leila Y. Mathers Charitable Foundation (C.J.W.), an Edward R. and Anne G. Lefler Center postdoctoral fellowship (M.S.R.), a Swiss National Science Foundation grant (D.K.), and an EMBO postdoctoral fellowship (C.B.).

Supporting Online Material
www.sciencemag.org/cgi/content/full/327/5964/463/DC1
Materials and Methods
SOM Text
Figs. S1 to S6
References

3 August 2009; accepted 7 December 2009
10.1126/science.1180067

Tuberculous Granuloma Induction via Interaction of a Bacterial Secreted Protein with Host Epithelium

Hannah E. Volkman,[1]* Tamara C. Pozos,[2]*† John Zheng,[2] J. Muse Davis,[3] John F. Rawls,[4,5] Lalita Ramakrishnan[6,7,8]‡

Granulomas, organized aggregates of immune cells, are a hallmark of tuberculosis and have traditionally been thought to restrict mycobacterial growth. However, analysis of *Mycobacterium marinum* in zebrafish has shown that the early granuloma facilitates mycobacterial growth; uninfected macrophages are recruited to the granuloma where they are productively infected by *M. marinum*. Here, we identified the molecular mechanism by which mycobacteria induce granulomas: The bacterial secreted protein 6-kD early secreted antigenic target (ESAT-6), which has long been implicated in virulence, induced matrix metalloproteinase–9 (MMP9) in epithelial cells neighboring infected macrophages. MMP9 enhanced recruitment of macrophages, which contributed to nascent granuloma maturation and bacterial growth. Disruption of MMP9 function attenuated granuloma formation and bacterial growth. Thus, interception of epithelial MMP9 production could hold promise as a host-targeting tuberculosis therapy.

Tuberculous infection begins with recruitment of monocytes to a peripheral infection site where they engulf mycobacteria and migrate to deeper tissues (*1*, *2*). Additional macrophages and other immune cells then aggregate with the infected cells to form granulomas (*3*). Granulomas, recognized as pathological hallmarks of tuberculosis for over a century, were thought to curtail infection by encasing mycobacteria (*4*). However, visualization of granuloma formation in transparent zebrafish larvae infected with *Mycobacterium marinum* (Mm) has revealed that the early granuloma serves to expand bacterial numbers (*5*, *6*). An infected macrophage induces granuloma formation by promoting recruitment of additional phagocytes (*6*). Upon its death, multiple newly arriving macrophages phagocytose it and thereby become infected. Concerted iteration of these processes makes the early granuloma a site for bacterial expansion (*6*). Mycobacteria direct these granuloma-forming processes via their region of difference–1 (RD1) virulence locus that encodes the ESAT-6 secretion system–1 (ESX-1) secretion system (*5*, *6*). The host factors coopted in RD1-mediated granuloma formation remain unknown.

In a host gene expression survey comparing zebrafish larvae infected with wild-type Mm (WT) or RD1-deleted Mm (ΔRD1) (*5*, *6*), we identified *matrix metalloproteinase 9* (*mmp9*) and *tissue inhibitor of metalloproteinase 2b* (*timp2b*) as being RD1-induced during granuloma formation at 5 days post infection (5 dpi) (Fig. 1, A and B; tables S1 to 4; and fig. S1, A and B). To control for ΔRD1's attenuated infection at 5 dpi (*5*), we confirmed RD1-dependent gene induction using higher ΔRD1 inoculations that produced similar bacterial burdens at 5 dpi with the expected paucity of ΔRD1 granulomas (*5*, *6*) (Fig. 1, A and C, and fig. S1C). At 1 dpi, only *mmp9* was induced, suggesting that *timp2b* induction at 5 dpi was a compensatory response to increased *mmp9* (Fig. 1D). Mmp9 is a gelatinase, and gelatin zymography confirmed that RD1-dependent *mmp9* mRNA expression resulted in increased Mmp9 gelatinase activity (Fig. 1E). In contrast, mRNA expression and activity of another gelatinase Mmp2 were not altered by infection (fig. S1A and Fig. 1E).

MMP9 is implicated in the pathogenesis of several inflammatory conditions (*7*, *8*) and is highly expressed in human tuberculosis as well as in the mouse model of tuberculosis (*9*–*12*) (table S1). In mice, MMP9 activity correlates to increased macrophage migration and granuloma formation; however, it is reported to be a host resistance factor, perhaps because its expression is associated with variable effects on infection in different genetic backgrounds (*10*). In humans, MMP9 clearly mediates susceptibility as its increased activity is correlated with worse outcomes (*9*). To test *mmp9*'s role in promoting granuloma formation and virulence, we knocked down its expression transiently with three modified antisense oligonucleotides (morpholinos) (*1*, *13*) (fig. S2). The morpholinos, singly or in combination, reduced gelatinase activity reliably up to 4 dpi with activity returning to control levels by 5 dpi (fig. S2). WT infection of morpholino-injected embryos (morphants) resulted in attenuated infection sharing several features of ΔRD1 infection of control embryos. First, morphants displayed reduced numbers of bacteria and granulomas, as well as increased host survival (Fig. 2, A to C). Second, kinetic analyses of granuloma formation in the morphants confirmed a specific granuloma-forming deficit (Fig. 2, D to F). We found a dynamic link between Mmp9 activity, granuloma formation, and bacterial expansion: Bacterial burdens and granuloma formation differed only up to 4 dpi, returning to control levels by 5 dpi contemporaneous with restoration of Mmp9 activity (Fig. 2, A to E, and fig. S2). Finally, although the RD1 locus promotes macrophage recruitment to nascent granulomas, it is not required for initial phagocyte migration to infecting bacteria when they are still extracellular (*5*, *6*). Similarly, *mmp9* morphants displayed normal macrophage migration to extracellular bacteria when injected into the hindbrain ventricle (fig. S3).

RD1 probably contributes to granuloma expansion through pleiotropic effects that include inducing apoptosis of infected macrophages and recruiting new uninfected macrophages (*5*, *6*, *14*–*16*). In contrast, Mmp9 was not required for RD1-induced cell death; morphant and control granulomas in WT infection contained similar numbers of TUNEL (terminal deoxynucleotidyl transferase–mediated deoxyuridine triphosphate nick end labeling)–positive cells, whereas control granulomas in ΔRD1 infection exhibited the expected reduction (*13*) (Fig. 2G). Thus RD1-induced apoptosis is Mmp9 independent and cannot mediate bacterial ex-

[1]Molecular and Cellular Biology Graduate Program, University of Washington, Seattle, WA 98155, USA. [2]Department of Pediatrics, University of Washington, Seattle, WA 98155, USA. [3]Immunology and Molecular Pathogenesis Graduate Program, Emory University, Atlanta, GA 30322, USA. [4]Department of Cell and Molecular Physiology, University of North Carolina, Chapel Hill, NC 27599, USA. [5]Department of Microbiology and Immunology, University of North Carolina, Chapel Hill, NC 27599, USA. [6]Department of Microbiology, University of Washington, Seattle, WA 98155, USA. [7]Department of Medicine, University of Washington, Seattle, WA 98155, USA. [8]Department of Immunology, University of Washington, Seattle, WA 98155, USA.

*These authors contributed equally to this work.
†Present address: Pediatric Infectious Diseases and Immunology, Children's Hospitals and Clinics of Minnesota, St. Paul, MN 55102, USA.
‡To whom correspondence should be addressed. E-mail: lalitar@u.washington.edu

www.sciencemag.org/cgi/content/full/327/5964/463/DC1

Supporting Online Material for

Identification of RACK1 and Protein Kinase Cα as Integral Components of the Mammalian Circadian Clock

Maria S. Robles, Cyril Boyault, Darko Knutti, Kiran Padmanabhan, Charles J. Weitz*

*To whom correspondence should be addressed. E-mail: cweitz@hms.harvard.edu

Published 22 January 2010, *Science* **327**, 463 (2010)
DOI: 10.1126/science.1180067

This PDF file includes:

Supporting Online Material

(Materials and Methods; Text, Figures S1 to S6, References.)

Materials and Methods

Mice and Tissue Collection C57BL/6J mice were entrained to a 12-12-h light-dark cycle for at least 10 days and then transferred to constant darkness. Mice were euthanized under infrared light, and tissues were dissected under light and frozen immediately in liquid nitrogen. Studies were performed in accordance with the protocol approved by the Harvard Medical School *Standing Committee on Animals*.

Fibroblast Cell Lines *Bmal1-Luc* circadian reporter fibroblasts: *Bmal1-Luc* mice carry a bacterial artificial chromosome (BAC) transgene, in which the coding exons and included introns were replaced with cDNA encoding firefly luciferase and the SV40 polyadenylation sequence. *Bmal1-Luc* immortalized cell line (BLi cells) was generated from these mice as follows. ~2cm tail was collected, minced, incubated in HBS containing 200 units/ml collagenase (Gibco) for 1 h at 37˚C. The dispersate was filtered through a cell strainer (40 μm, Falcon), and the cells were then pelleted by centrifugation. The pellet was resuspended in DMEM containing 9% FBS, and the cells were plated onto 10-cm culture plates. Proliferating primary fibroblasts were expanded and then immortalized using *pBABE-puro-SV40T* retrovirus (*S1*) followed by Puromycin resistance selection and anti-mycoplasm treatment (BM-cyclin, Roche). BLi is a clonal cell line derived from mice carrying *Bmal1-Luc* in a wildtype background; the *Mop3*$^{-/-}$*-Luc* immortalized cell line (MLi cells) was derived in the same way but from *Bmal1-Luc;*

Bmal1$^{-/-}$ (*Mop3*$^{-/-}$) mice. Stable cell lines expressing FH-BMAL1 (Endogneous promoter, FH-BMAL1; EFH cells) were generated by transfecting BLi cells with an expression plasmid in which a proximal 1-kb fragment of the *Bmal1* promoter is linked to a cDNA encoding FH-BMAL1 (*pBS/Neo-endo/FH-Bmal1*). After 48 h, stable clones were selected with G418 (500 μg/ml). Surviving clones (2-3 weeks) were pooled.

Sucrose Density Gradient Centrifugation Cell or tissue lysates (50 mM Hepes pH 7.5, 150 mM NaCl, 10 mM EDTA, 1 mM DTT, 1% NP-40) were layered on a 5-45% (w/v) sucrose gradient (Biocomp Gradient Master) in 50mM Hepes, 150 mM NaCl, 10 mM EDTA, and 0.1% NP40. Lysates were sedimented at 182,000 g for 15 h at 3˚C. Molecular mass standards, run in parallel, were Alcohol Dehydrogenase (150 kDa), Ferritin (440 kDa), and Thyroglobulin (669 kDa).

Adenoviruses and Preparation of Cells for Purification of BMAL1 Protein Complexes Parental vectors used were *pAdlox* (*S2*) for protein over-expression or *pAdSUPER* (*S3*) for shRNA expression. Recombinant viruses were passaged through CRE8 cells >3x, then large-scale batches were generated yielding titers of typically 0.5-2x10^{9} pfu/ml. *AdV-eFH-Bmal1* expresses FH-BMAL1 driven by a 1kb *Bmal1* promoter fragment. For proteomics experiments, 3x10^{6} MLi cells were plated on 2x15cm plates and infected (M.O.I. = 10) with *AdV-eFH-Bmal1* (Polybrene, 8 μg/ml, Sigma). 48h after infection, cells were treated with 100 μM forskolin for 2 h, then fresh medium was added. 16 h after synchronization, cells were washed once with PBS, detached with Cell Stripper (Mediatech), pelleted by centrifugation, washed with cold PBS, pelleted by centrifugation, resuspended in cold PBS, pelleted by centrifugation, and stored at -80°C.

LC-MS/MS Mass Spectrometry Samples were analyzed at the Taplin Biological Mass Spectrometry Facility, Harvard Medical School. Excised gel lanes were cut into seven pieces. Gel pieces were then subjected to a modified in-gel trypsin digestion procedure (*S4*). Gel pieces were washed, dehydrated with acetonitrile for 10 min followed by removal of acetonitrile, and then dried in a speed-vac. Rehydration of the gel pieces was with 50 mM ammonium bicarbonate solution containing 12.5 ng/µl modified sequencing-grade trypsin (Promega) at 4ºC. After 45 min, excess trypsin solution was removed and replaced with 50 mM ammonium bicarbonate sufficient to cover the gel pieces. Samples were then incubated overnight at 37ºC. Peptides were extracted by removing the ammonium bicarbonate solution and washing once with a solution containing 50% acetonitrile and 5% acetic acid. The extracts were then dried in a speed-vac (~1 hr). The samples were then stored at 4ºC until analysis.

On the day of analysis the samples were reconstituted in 5-10 µl of HPLC solvent A (2.5% acetonitrile, 0.1% formic acid). A nano-scale reverse-phase HPLC capillary column was created by packing 5 µm of C18 spherical silica beads into a fused silica capillary (100 µm inner diameter x ~12 cm in length) with a flame-drawn tip (*S5*). After equilibrating the column, each sample was loaded via a Famos auto sampler (LC Packings) onto the column. A gradient was formed, and peptides were eluted with increasing concentrations of solvent B (97.5% acetonitrile, 0.1% formic acid). As peptides eluted they were subjected to electrospray ionization and then entered into an LTQ linear ion-trap mass spectrometer (ThermoFisher). Peptides were detected, isolated, and fragmented to produce a tandem mass spectrum of specific fragment ions for each peptide. Peptide sequences (and thus protein identity) were determined by

matching protein databases with the acquired fragmentation pattern by the software program Sequest (ThermoFisher). Spectral matches were manually examined and multiple identified peptides per protein were required.

Cell Fractionation Cells were lysed (15 mM NaCl, 60 mM KCl, 12% [w/v] sucrose, 2 mM EDTA, 0.5 mM EGTA, 0.65 mM spermidine, 1 mM DTT, 0.05% Triton X-100, protease inhibitor cocktail EDTA-free [Roche], phosphatase inhibitor cocktails I and II [Sigma]). Nuclei were pelleted (13,000 g, 15 min), and the supernatant (cytoplasmic fraction) was stored at -80°C. Nuclei were washed 3X in lysis buffer and resuspended in 100 mM HEPES pH 7.4, 200 mM NaCl, 0.5% NP40, with protease and phosphatase inhibitor cocktails as above. The suspension was sonicated and then centrifuged at 10,000 g, and the supernatant (nuclear fraction) was collected.

Antibodies and Western Blotting Anti-BMAL1 antiserum was a gift of Paolo Sassone-Corsi (University of California, Irvine). Antibodies against the following proteins were obtained from the indicated suppliers: □-TUBULIN (Sigma, 1:5000), RACK1 (BD Transduction, 1:1000 or Abcam, 1:1000), PKC□ (Santa Cruz, 1:1000), RNA Pol II CTD (Abcam, 1:5000), FLAG M2 (Sigma, 1:5000), PER2 (BD Transduction, 1:1000), HRP-conjugated secondary antibodies (Amersham, 1:5000). Extracts (5-10 □g of protein) were resolved by SDS–PAGE, blotted onto nitrocellulose (Amersham), and analyzed by enhanced chemiluminescence (Amersham).

Co-Immunoprecipitation Cells and tissues: For RACK1, 2 μg of anti-RACK1 IgM or control IgM was incubated with 500 μg of cell extract (overnight, 4^{o}C), then with rabbit anti-IgM (1 h, 4^{o}C), followed by incubation with Protein-G sepharose (Amersham). For FH-BMAL1, 20 μl of anti-FLAG M2 affinity gel (Sigma) slurry was incubated with

500 µg of cell extract (overnight, 4°C). Sucrose gradient fractions: fractions (0.5 ml), supplemented with protease and phosphatase inhibitors, were incubated with RACK1 IgM or control IgM antibodies (2 ug) linked to Protein-G sepharose (overnight, 4˚C). Beads were washed 3X (1 ml, 0.05% NP-40), and protein complexes were eluted in Laemmli buffer and resolved on SDS-PAGE.

Recombinant Protein Production and In Vitro Binding Assays *E. coli* strain BL21 was transformed by *pGEX4T1-RACK1* and grown to OD_{600} = 0.7 before induction by 0.1 mM IPTG for 3 h at 37°C. Cells were centrifuged at 6,000 g for 10 min, sonicated in lysis buffer (100 mM HEPES pH7.4, 1% triton, 500 mM NaCl, 5 mM 2-mercaptoethanol, protease inhibitor cocktail, complete EDTA-Free). After centrifugation at 12,000 g for 30 min, the supernatant was applied to a glutathione sepharose column (Sigma) for 2 hours at 4°C, then washed in 30 column volumes of lysis buffer. GST-RACK1 was eluted with reduced glutathione (Sigma) in 100 mM HEPES pH7.4, 150 mM NaCl, 5 mM 2-mercaptoethanol, with anti-protease. The protein concentration was measured, and 10% glycerol was added to the solution before freezing for storage at -80°C. For MBP-C2 expression, *E. coli* BL21 cells were grown to OD_{600} = 0.7 before induction with 0.1 mM IPTG for 3 h at 37°C. Cells were collected by centrifugation and sonicated in 100 mM HEPES pH7.4, 0.5% Triton, 500 mM NaCl, 5 mM 2-mercaptoethanol and anti-proteases complete, EDTA free. After centrifugation at 12,000 g for 30 min, the supernatant was applied to amylose resin for 2 h at 4°C. The resin was washed in 100 mM HEPES pH7.4, 1 M NaCl and 5 mM 2-mercaptoethanol, and the fusion protein was eluted in 100 mM HEPES pH 7.4, 200 mM NaCl, 10 mM maltose, 5 mM 2-mercaptoethanol. In some cases resin was transferred directly to

Laemmli buffer for SDS-PAGE analysis of the bound proteins. The protein concentration was measured, and 10% glycerol was added to the solution before freezing and storage at -80°C.

For in vitro protein interaction experiments, ^{35}S-labeled full-length CLOCK, BMAL1, and MYOD proteins were synthesized individually or together in vitro by using the TnT quick coupled transcription/translation systems (Promega). 1 µl of a 50-µl reaction was diluted in 500 µl of binding buffer (100 mM Hepes, pH7.4, 150 mM NaCl, 10% Glycerol, 0.1% Triton, antiproteases) for addition to GST-RACK1 beads. After 2 h at 4°C, the beads were washed 3X in binding buffer, and retained proteins were resolved on SDS-PAGE and visualized by autoradiography. For MBP-C2 binding, proteins produced as above were incubated with MBP-C2-amylose beads in binding buffer [100 mM Hepes, pH7.4, 150 mM NaCl, 10% Glycerol, 0.1% Triton, antiprotease (Roche) EDTA free] for 2 h at 4°C. The beads were washed 3X in binding buffer, and retained proteins were resolved on SDS-PAGE for visualization by autoradiography.

Transactivation Assay 293T cells were transfected with Lipofectamine-Plus (GibcoBRL) or FuGene HD transfection reagent (Roche), and transactivation assays were performed essentially as described (*S6*), using 500 µg of total DNA per well. For expression in mammalian cells, C2 peptide cDNA was subcloned into *pcDNA3.1-Flag* (Invitrogen) by PCR from the *pMAL* vector (News England Biolabs) using the following primers:

5’ GCG GGA TCC GTT GTT GTA AGA GAT GCT AAA AAT CTG GTA and 5’ CGG CTC GAG TCA TCA GGG CAC ATT GAA GTA TTC ACC CTC TTC CTG

and ligated into *BamHI - XhoI* sites. The insert sequence was verified.

In Vitro Phosphorylation Assay In vitro-synthesized BMAL1 was incubated in phosphorylation buffer (20 mM Hepes pH 7.4; 10mM $MgCl_2$; 0.1mM $CaCl_2$; 100μM ATP and trace □-^{32}P ATP (Perkin Elmer), supplemented with diacylglycerol and phosphatidylserine (Avanti Polar Lipids). PKC□, PKC□I, or PKC□II (Sigma) was added as recommended by the manufacturer. For kinase positive control assays, histone H1 (Sigma) was added to a final concentration of 200 □g/ml, as recommended in the kinase instructions. The reaction was stopped by addition of Laemmli buffer and analyzed by SDS-PAGE. After fixation and drying, the gel was exposed overnight at room temperature, and phosphor images were obtained (Molecular Dynamics Storm 840; ImageQuant 5.0).

RNA interference against RACK1 shRNA vectors were constructed by ligating synthetic oligonucleotides into the recombination *pAdlox-SUPER* vector (made by replacing the *XbaI/KpnI* fragment of *pAdlox/prm* with *XbaI/KpnI* of *pSUPER*). The insert sequence was verified. Oligomers (Integrated DNA Technologies) for RACK1 shRNA:

R1 sense : 5’ ATC CCC GAG ACA AGA CCA TAA AGT TTT CAA GAG AAA CTT TAT GGT CTT GTC TCT TTT TGG AAA

R1 antisense : 5’GCT TTT CCA AAA AGA GAC AAG ACC ATA AAG TTT CTC TTG AAA ACT TTA TGG TCT TGT CTC GGG

R1 scr sense : 5’GAT CCC CGA GAC AAC GAC ATA AAG TTT TCA AGA GAA ACT TTA TGT CGT TGT CTC TTT TTG GAA A

R1 scr antisense : 5’AGC TTT TCC AAA AAG AGA CAA CGA CAT AAA GTT TCT CTT GAA AAC TTT ATG TCG TTG TCT CGG G

R3 sense : 5'GAT CCC CGC AAG ATC ATT GTA GAT GAT TCA AGA GAT CAT CTA CAA TGA TCT TGC TTT TTG GAA A

R3 antisense : 5'AGC TTT TCC AAA AAG CAA GAT CAT TGT AGA TGA TCT CTT GAA TCA TCT ACA ATG ATC TTG CGG G

R3 mut sense : 5'GAT CCC CGC AAG ATT ACT GTA GAT GAT TCA AGA GAT CAT CTA CAG TAA TCT TGC TTT TTG GAA A

R3 mut antisense : 5'AGC TTT TCC AAA AAG CAA GAT TAC TGT AGA TGA TCT CTT GAA TCA TCT ACA GTA ATC TTG CGG G

R5 sense : 5'GAT CCC CCA AGC ACC TCT ACA CTT TAT TCA AGA GAT AAA GTG TAG AGG TGC TTG TTT TTG GAA A

R5 antisense : 5'AGC TTT TCC AAA AAC AAG CAC CTC TAC ACT TTA TCT CTT GAA TAA AGT GTA GAG GTG CTT GGG G

R5 mut sense : 5'GAT CCC CCA AGC ACC TAC TCA CTT TAT TCA AGA GAT AAA GTG AGT AGG TGC TTG TTT TTG GAA A

R5 mut antisense : 5'AGCT TTT CCA AAA ACA AGC ACC TAC TCA CTT TAT CTC TTG AAT AAA GTG AGT AGG TGC TTG GGG

RNA interference against PKC□. SiRNA were electroporated with Nucleofector system (Amaxa, Solution VII, Lonza). Oligomers (Integrated DNA Technologies) were designed to be highly specific for the PKC□ isozyme:

P1 sense : 5' GGA GCA CAG GGU UCG UAG ACA AUC C

P1 antisense : 5' GGA UUG UCU ACG AAC CCU GUG CUC CUU

P1 mut sense : 5' GAA ACA CAA AGU UCG UAC ACA AUC C

P1 mut antisense : 5' GGA UUG UGU ACG AAU UCU UUG UUU CUU

P2 sense : 5’ CAA CGA CCU GCC AGC UUC UGC UCA G

P2 antisense : 5’ CUG AGC AGA AGC UGG CAG GUC GUU GUU

P2 mut sense : 5’ GAA CAA AAU GCC AGC UUC UGC UCA G

P2 mut antisense : 5’ CUG AGC AGA AGC UGG CAU UUU GUU CUU

P3 sense : 5’ CAG GGA GAU CCA ACC ACC AUU CAA G

P3 antisense : 5’ CUU GAA UGG UGG UUG GAU CUC CCU GUU

P3 mut sense : 5’ GAA UUA CAU CCA ACC ACC AUU CAA G

P3 mut antisense : 5’ UUG AAU GGU GGU UGG AUG UAA UUC UU

Real-Time Monitoring of Circadian Oscillations BLi cells at 90% confluence were synchronized by addition of DMEM containing 10 μM forskolin. After 2 h, the medium was changed to DMEM with 10% FBS, 100 U/ml penicillin, 100 □g/ml streptomycin, and 250 □M d-Luciferin. Bioluminescence was continuously recorded (LumiCycle, Actimetrics) and analyzed as described [W.-N. Zhao *et al*., *Nat. Cell Biol*. **3**, 268 (2007)].

SOM Text

Presence of RACK1 and PKC□ in ~400-kD BMAL1 protein complexes To characterize nuclear RACK1 and PKC□ in relation to BMAL1 complexes, we performed sucrose density gradient centrifugation of nuclear extracts from mouse tissues or BLi fibroblasts harvested during the negative feedback phase of the circadian cycle and monitored the fractions for the presence of the proteins by Western blotting. From lung, BMAL1 and RACK1 largely co-sedimented, with the great majority of both proteins present in the 200-400-kD range (Fig. S3A). From fibroblasts, BMAL1, RACK1 and

PKC largely co-sedimented, with the majority of all three proteins also found in the 200-400-kD range; in contrast, RNA Polymerase II, as expected, was found in much larger complexes (Fig. S3B).

Many proteins might be found in complexes of this size range, so to determine if the co-sedimentation of RACK1 and BMAL1 was at least in part due to the presence of the two proteins in the same complex (as opposed to coincidental migration in sucrose gradients), we pooled three contiguous sucrose gradient fractions centered at 400 kD (underlined in Fig. S3B), immunoprecipitated RACK1, and probed for BMAL1. BMAL1 from the pooled fractions specifically co-immunoprecipitated with RACK1 (Fig. S3C), indicating that the two proteins are present in complexes of about 400 kD. Similarly, to determine if the co-sedimentation of PKC and BMAL1 was at least in part due to the presence of the two proteins in the same complex, we performed a sucrose gradient fractionation of nuclear extracts from EFH fibroblasts and immunoprecipitated FH-BMAL1 with an anti-FLAG antibody from fractions centered at 400 kD. PKC from the fractions specifically co-immunoprecipitated with FH-BMAL1, indicating that the two proteins are present in a complex (Fig. S3D). Thus RACK1 and PKC are constituents of one or more ~400-kD BMAL1 nuclear protein complexes, suggesting that they work together to regulate BMAL1 function.

Action of RACK1 as a suppressor of CLOCK-BMAL1 activity unlikely to be accounted for by an effect on CLOCK or BMAL1 stability RACK1 has been reported to target the transcription factor hypoxia-inducible factor-1 (HIF-1) for proteasomal degradation (*S7*). To determine if the inhibition of CLOCK-BMAL1 activity by RACK1 might result from an effect of RACK1 on stability, we monitored the decay

rates of BMAL1 and CLOCK in cycloheximide-treated fibroblasts in the presence or absence of expressed RACK1. We found no effect of RACK1, but the half-life of RACK1 itself under these conditions was much shorter than the half-lives of BMAL1 and CLOCK, precluding a test of RACK1 (not shown). As an alternative, we monitored the steady-state levels of expressed BMAL1 or CLOCK in the presence or absence of expressed RACK1. RACK1 had no detectable effect on CLOCK, but it produced a significant 25-30% decline in the steady-state level of BMAL1 (Fig. S4A; $P < 0.02$, *t-test*).

To examine how the effect of RACK1 on BMAL1 levels might relate to the inhibition of CLOCK-BMAL1 activity by RACK1, we performed luciferase assays of CLOCK-BMAL1 transcriptional activity in the presence of increasing amounts of expressed RACK1 while monitoring BMAL1 protein in the same cells. Increasing expression of RACK1 produced a shallow decline in BMAL1 steady-state levels, from 100% to 80% of baseline, whereas it led to a much steeper decline of CLOCK-BMAL1 transcriptional activity, from 100% to 30% of baseline (Fig. S4B). Low RACK1 expression levels with no detectable effect on steady-state BMAL1 levels nonetheless produced a significant >50% inhibition of CLOCK-BMAL1 activity (Fig. S4B). Although we cannot exclude a highly non-linear relationship between BMAL1 levels and CLOCK-BMAL1 activity, these results suggest that the decrease in BMAL1 steady-state levels produced by RACK1 is unlikely to account for its inhibition of CLOCK-BMAL1 transcriptional activity.

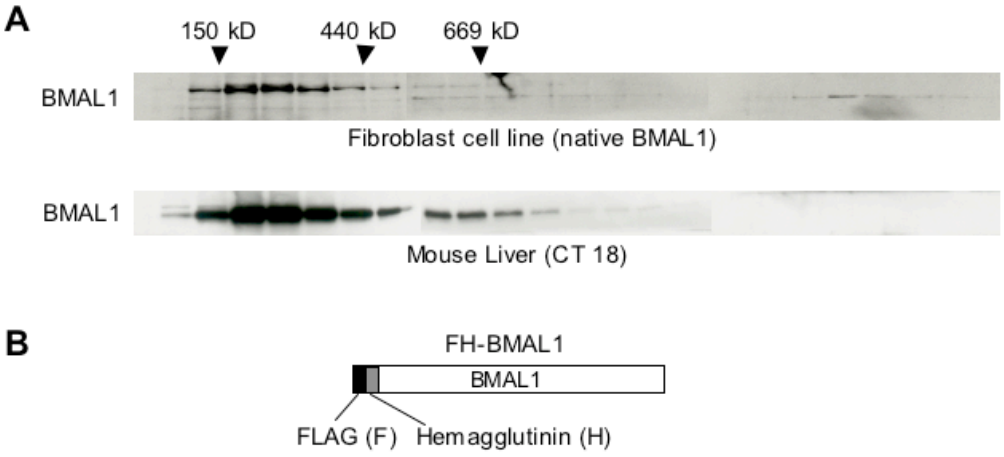
A
150 kD
440 kD
669 kD
BMAL1
Fibroblast cell line (native BMAL1)
BMAL1
Mouse Liver (CT 18)
B
FH-BMAL1
BMAL1
FLAG (F)
Hemagglutinin (H)

Fig. S1

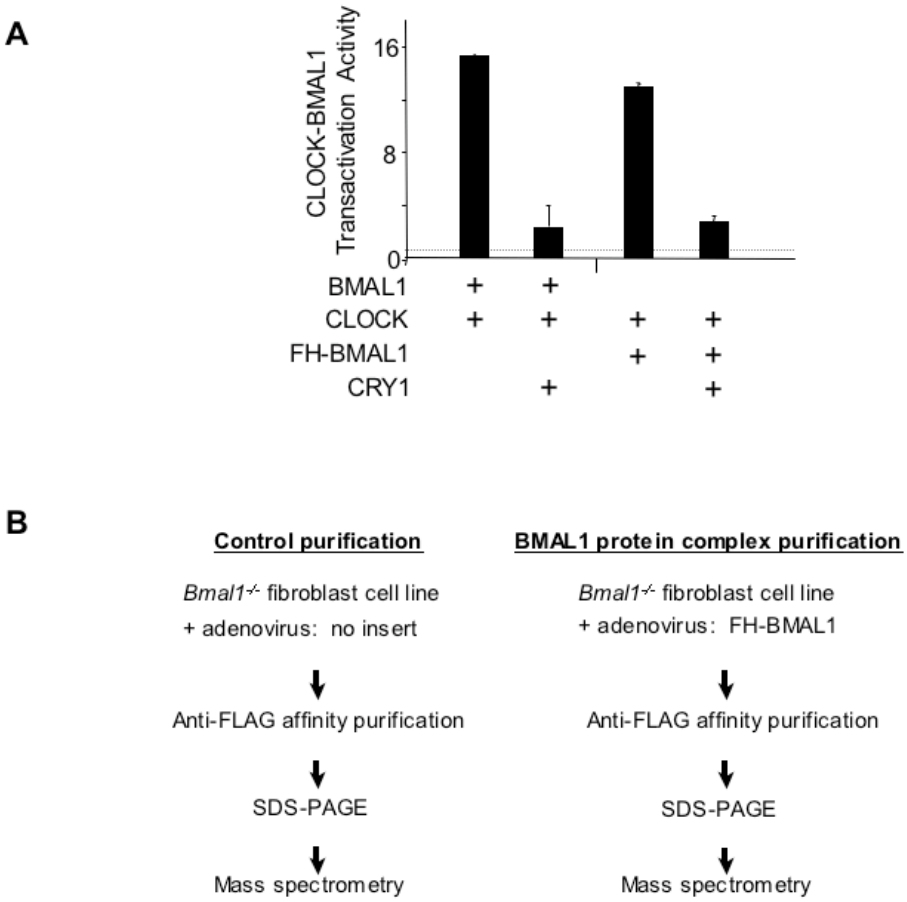
A
CLOCK-BMAL1 Transactivation Activity
16
8
0
BMAL1 + +
CLOCK + + + +
FH-BMAL1 + +
CRY1 + +
B
Control purification
Bmal1-/- fibroblast cell line
+ adenovirus: no insert
Anti-FLAG affinity purification
SDS-PAGE
Mass spectrometry
BMAL1 protein complex purification
Bmal1-/- fibroblast cell line
+ adenovirus: FH-BMAL1
Anti-FLAG affinity purification
SDS-PAGE
Mass spectrometry

Fig. S2

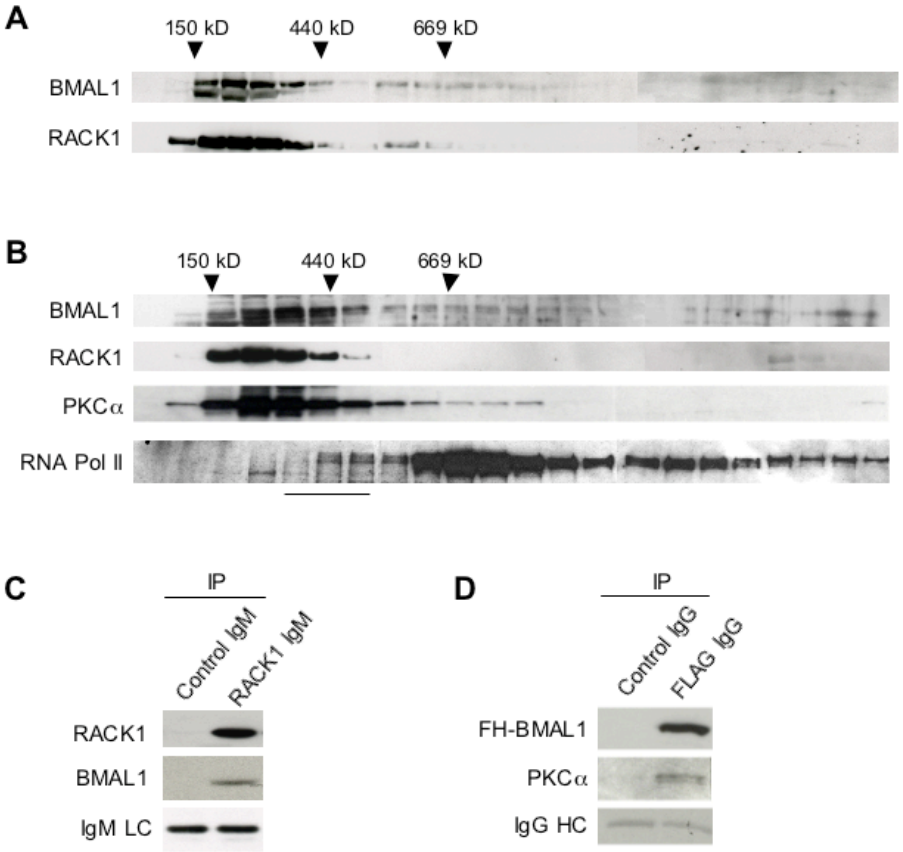
A
150 kD
440 kD
669 kD
BMAL1
RACK1
B
150 kD
440 kD
669 kD
BMAL1
RACK1
PKCα
RNA Pol II
C
IP
Control IgM
RACK1 IgM
RACK1
BMAL1
IgM LC
D
IP
Control IgG
FLAG IgG
FH-BMAL1
PKCα
IgG HC

Fig. S3

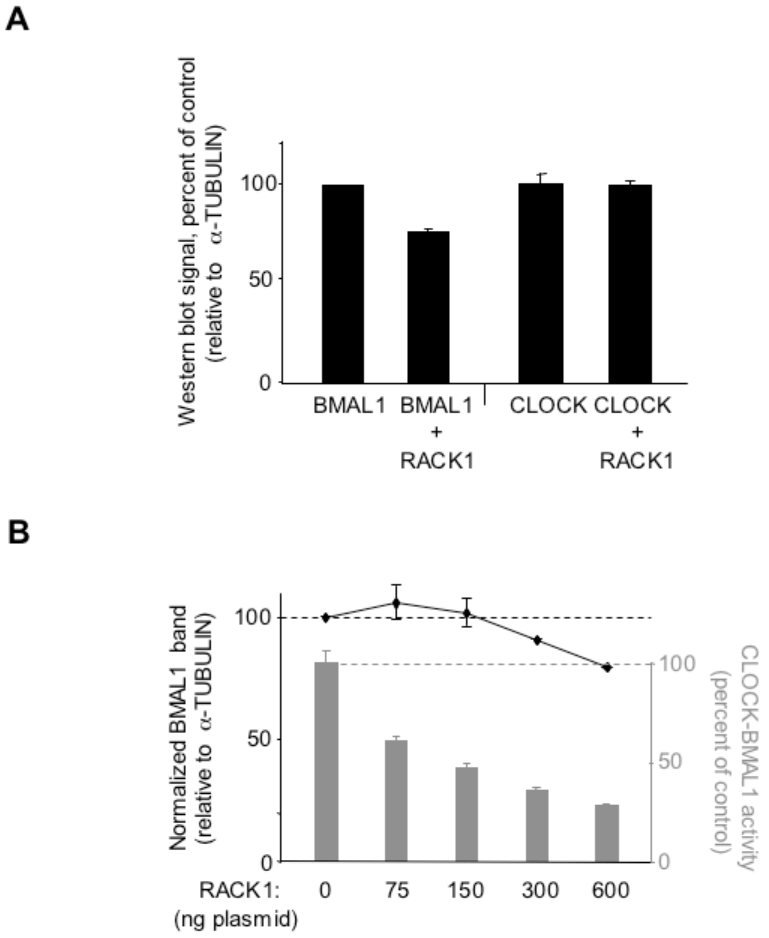
A
Western blot signal, percent of control
(relative to α-TUBULIN)
100
50
0
BMAL1
BMAL1
+
RACK1
CLOCK
CLOCK
+
RACK1
B
Normalized BMAL1 band
(relative to α-TUBULIN)
100
50
0
CLOCK-BMAL1 activity
(percent of control)
100
50
0
RACK1:
(ng plasmid)
0
75
150
300
600

Fig. S4

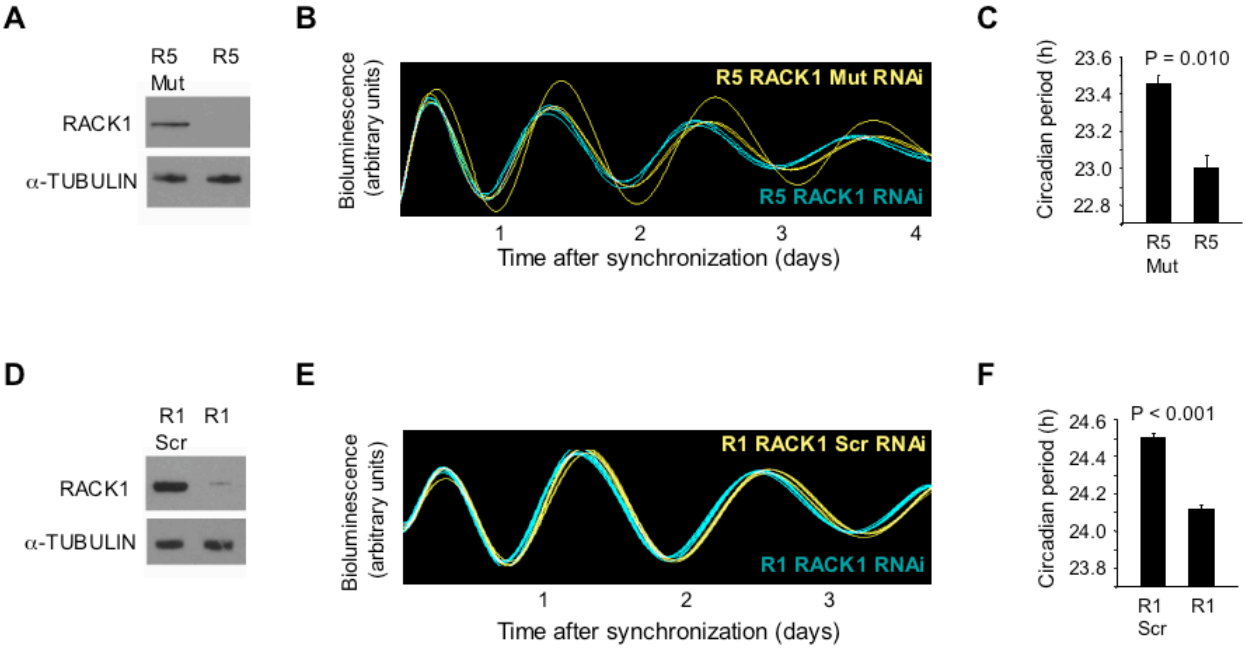
A
R5
Mut
R5
RACK1
α-TUBULIN
B
Bioluminescence (arbitrary units)
R5 RACK1 Mut RNAi
R5 RACK1 RNAi
1
2
3
4
Time after synchronization (days)
C
Circadian period (h)
23.6
23.4
23.2
23.0
22.8
P = 0.010
R5
Mut
R5
D
R1
Scr
R1
RACK1
α-TUBULIN
E
Bioluminescence (arbitrary units)
R1 RACK1 Scr RNAi
R1 RACK1 RNAi
1
2
3
Time after synchronization (days)
F
Circadian period (h)
24.6
24.4
24.2
24.0
23.8
P < 0.001
R1
Scr
R1

Fig. S5

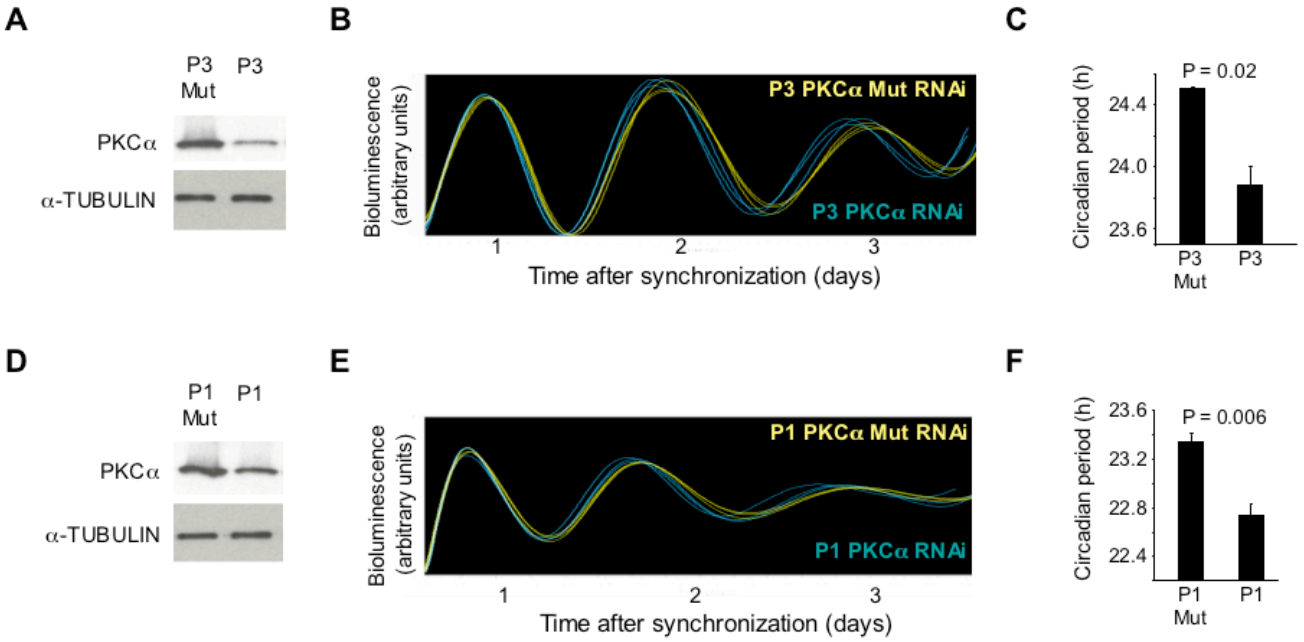
A
P3 Mut
P3
PKCα
α-TUBULIN
B
Bioluminescence (arbitrary units)
P3 PKCα Mut RNAi
P3 PKCα RNAi
1
2
3
Time after synchronization (days)
C
Circadian period (h)
P = 0.02
24.4
24.0
23.6
P3 Mut
P3
D
P1 Mut
P1
PKCα
α-TUBULIN
E
Bioluminescence (arbitrary units)
P1 PKCα Mut RNAi
P1 PKCα RNAi
1
2
3
Time after synchronization (days)
F
Circadian period (h)
P = 0.006
23.6
23.2
22.8
22.4
P1 Mut
P1

Fig. S6

SOM Figure Legends

Fig. S1 Detection of BMAL1 protein complexes and design of tandem epitope-tagged BMAL1 protein. (**A**) Sucrose density gradient sedimentation (5-45% sucrose, left-to-right) of BMAL1 protein complexes from mouse fibroblasts (top) or mouse liver nuclei (bottom). Image shows Western blot probed with anti-BMAL1 to monitor endogenous BMAL1 in sucrose gradient fractions. Positions and masses of marker proteins are indicated at the top. (**B**) Diagram of FH-BMAL1, in which the FLAG-Hemagglutinin (FH) tandem affinity purification tag has been fused to the BMAL1 N-terminus.

Fig. S2 Proteomics strategy to identify constituents of BMAL1 protein complexes. (**A**) Similarity of FH-BMAL1 and native BMAL1 in transcriptional activity and suppression by CRY1. Data show transactivation of a luciferase reporter gene from *Per1* E-boxes in mouse fibroblasts (mean and S.D.; N ≥ 3). Mean luciferase activity after transfection of expression vector lacking *Clock* or *Bmal1* cDNA inserts was set to 1 (dashed line). +, transfection of expression plasmid with insert encoding the indicated protein. (**B**) Diagram summarizing the immunoaffinity purification of BMAL1 protein complexes.

Fig. S3 Presence of RACK1 and PKC□ in ~400-kD BMAL1 protein complexes. (**A**) Co-sedimentation of BMAL1 (top) and RACK1 (bottom) in sucrose density gradient analysis of mouse lung nuclear extract. Western blots of fractions are displayed as in Fig. 1. (**B**) Co-sedimentation of BMAL1, RACK1, and PKC□, but not RNA Pol II, in sucrose density gradient analysis of BLi fibroblast nuclear extract. Western blots of

fractions are displayed as in Fig. 1. Bar at bottom marks fractions pooled for immunoprecipitation analysis in (C). (**C**) Co-immunoprecipitation of BMAL1 with RACK1 from sucrose gradient fractions centered at ~400 kD. Fractions are marked at bottom of (B). Immunoprecipitates from control IgM or RACK1 IgM probed with antibodies for the proteins indicated at left. IgM LC, Immunoglobulin M light chain. (**D**) Co-immunoprecipitation of PKC with FH-BMAL1 from sucrose gradient fractions (EFH fibroblasts) centered at ~400 kD. Immunoprecipitates from control IgG or anti-FLAG IgG (FH-BMAL1) probed with antibodies for the proteins indicated at left. IgG HC, Immunoglobulin G heavy chain.

Fig. S4 Reduction of steady-state BMAL1 level by RACK1 unlikely to account for RACK1 inhibition of CLOCK-BMAL1 activity. (**A**) Steady-state levels of BMAL1 and CLOCK relative to -TUBULIN (mean and S.E.M.), as determined from Western blots, in the presence or absence of expressed RACK1 (as indicated; N = 6 for each). 293T cells were transfected (as described for the luciferase transactivation assays) with cDNAs encoding full-length CLOCK, BMAL1, and/or RACK1, as indicated, in the expression plasmid *pcDNA3.1-Flag* (Invitrogen). (**B**) Effect of RACK1 on steady-state BMAL1 level and CLOCK-BMAL1 transcriptional activity in the same cells. Curve at top (black line) shows relative steady-state level of BMAL1 as a function of increasing expression of RACK1. Gray bars show CLOCK-BMAL1 transactivation of a luciferase reporter from *Per1* E-boxes in the same cells.

Fig. S5 Confirmation of short circadian period length caused by depletion of endogenous RACK1. Shown are data following adenoviral delivery of either of two additional, non-overlapping shRNAs (**A-C** and **D-F,** respectively). (**A**) Western blot showing the effect of control shRNA (R5 mut, three point-mutations in 22-nt core sequence) or RACK1 shRNA (R5) on steady-state level of endogenous RACK1. □-TUBULIN, loading control. (**B**) Real-time circadian oscillations of bioluminescence in synchronized circadian reporter BLi fibroblasts after adenoviral delivery of R5 shRNA against RACK1 (blue) or corresponding mutated control shRNA (yellow). Traces from three independent cultures are shown for each. (**C**) Mean circadian period of fibroblasts expressing R5 Mut control or R5 RACK1 shRNA (mean +/- S.E.M.; N = 3 for each; *t-test*, two-tailed). (**D-F**) Data for control shRNA (S1 scr, scrambled 22-nt core sequence) or effective RACK1 shRNA (S1) displayed as above.

Fig. S6 Confirmation of short circadian period length caused by depletion of endogenous PKC□. Shown are data following electroporation of either of two additional, non-overlapping siRNAs (**A-C** and **D-F,** respectively). (**A**) Western blot showing the effect of control siRNA (P3 mut, three point-mutations in 22-nt core sequence) or PKC□ siRNA (P3) on steady-state level of endogenous PKC□. Depletion was ~70%. □-TUBULIN, loading control. (**B**) Real-time circadian oscillations of bioluminescence in synchronized circadian reporter BLi fibroblasts after electroporation of P3 siRNA against RACK1 (blue) or corresponding mutated control siRNA (yellow). Traces from three independent cultures are shown for each. (**C**) Mean circadian period of fibroblasts expressing P3 Mut control or P3 PKC□ siRNA (mean +/- S.E.M.; N = 3 for each; *t-test*,

two-tailed). (**D-F**) Data for control siRNA (P1 mut, three point-mutations in 22-nt core sequence) or effective PKC siRNA (P1) displayed as above. In this case depletion was ~50%.

SOM References

S1. J.J. Zhao *et al*. *Cancer Cell* **3**, 483 (2003).

S2. S. Hardy et al., *Virol.* **71**,1842 (1997).

S3. S.N. Schreiber, D. Knutti, K. Brogli, T. Uhlmann, A. Kralli. *J. Biol. Chem*. **278**, 9013 (2003).

S4. A. Shevchenko, M. Wilm, O. Vorm, M. Mann. *Anal. Chem.* **68**, 850 (1996).

S5. J. Peng, S.P. Gygi. *J. Mass Spec*. **36**, 1083 (2001).

S6. W.N. Zhao *et al*., *Nat. Cell Biol*. **3**, 268 (2007).

S7. Y.V. Liu, G.L. Semenza. *Cell Cycle* **6**, 656 (2007).